*Benjamin U. Oreko[1] , Moses T. Ogundele[1], Silas O. Okuma[2]**

[1]Department of Mechanical Engineering, Federal University of Petroleum Resources, Effurun, Nigeria

[2]Department of Mechanical Engineering, Nigeria Maritime University, Okerenkoko, Nigeria

Scientific paper
ISSN 0351-9465, E-ISSN 2466-2585
https://doi.org/10.62638/ZasMat1831

Zastita Materijala 67 ()
(2026)

Electrochemical assessment of corrosion resistance of PWHTUNSG10350 carbon steel weld in simulated seawater

ABSTRACT

This study investigates the effect of post-weld heat treatment (PWHT) on the corrosion behavior of carbon steel (CS) welded pipe in a chloride-containing brine environment at 25 °C. The corrosion performance of the as-welded (control) specimen was compared with that of PWHT-treated specimens at 300 °C, 450 °C, and 650 °C using gravimetric (mass-loss) measurements and electrochemical techniques, including open-circuit potential (OCP), potentiodynamic polarization (PDP), and electrochemical impedance spectroscopy (EIS).Mass-loss results obtained over 120 h of immersion showed that the as-welded specimen experienced the highest degradation. A rapid increase in weight loss was observed during the early exposure period (up to approximately 70 h), followed by a reduction in the mass-loss rate for all samples at longer immersion times. This behavior is attributed to the formation of a protective surface film. Similarly, the corrosion rates decreased with increasing immersion time, likely due to the accumulation of corrosion products that partially inhibited further attack.OCP measurements revealed that the PWHT-treated samples shifted toward more positive potentials relative to the as-welded condition, indicating improved surface stability associated with oxide-layer formation. PDP measurements further confirmed the enhanced corrosion resistance after PWHT, with corrosion rates reduced to 0.126, 0.0864, and 0.0148 mm·yr^{-1} for specimens treated at 300 °C, 450 °C, and 650 °C, respectively. The EISNyquist plots showed an increase in charge-transfer resistance with increasing PWHT temperature, accompanied by a decrease in double-layer capacitance, indicating improved interfacial protection. SEM observations supported the electrochemical and gravimetric results: the as-welded surface exhibited localized pitting, whereas PWHT promoted microstructural evolution toward tempered martensite and grain growth, resulting in significantly improved corrosion resistance, particularly for the PWHT-treated specimen at 650 °C. Overall, PWHT, especially at 650 °C, markedly enhanced the corrosion resistance of carbon steel weldments in chloride-containing environments

Keywords: *Carbon steel weld, weldability, PWHT, embrittlement, susceptibility*

1. INTRODUCTION

UNSG10350 carbon steel has a wide range of applications in oil and gas infrastructure, including pipelines and pressure vessels, due to its favorable mechanical properties, good weldability, and cost-effectiveness [1, 2]. Carbon steel is the most commonly used steel in the oil and gas industry because of its high strength, weldability, and durability; however, it is highly susceptible to corrosion, particularly in marine and highly aggressive environments [3–5].

Marine and subsea environments containing high concentrations of chloride ions present significant corrosion challenges to structural components. The high electrical conductivity of seawater, resulting from the presence of aggressive chloride ions, combined with variations in oxygen content and temperature, creates highly corrosive conditions in offshore applications. Welded structures exposed to such environments are especially vulnerable to corrosion, as the heterogeneous heat-affected zone (HAZ) often serves as a preferential site for localized attack. Seawater and industrial atmospheres rich in chloride ions (Cl^-) promote corrosive processes such as pitting corrosion, stress corrosion cracking (SCC), and hydrogen embrittlement, particularly in welded joints where microstructural changes and

*Corresponding author: Silas O. Okuma
E-mail: silasoseme@gmail.com
Rad primljen: 29.03.2026.
Rad korigovan: 11.05.2026.
Rad prihvaćen: 06.07.2026.

residual stresses contribute to localized weaknesses [6–8].

Welding is an essential process for joining steel materials; however, it significantly alters the microstructure of the steel, especially within the heat-affected zones. These regions become more susceptible to pitting corrosion, hydrogen embrittlement, and stress corrosion cracking [9–11]. Inhomogeneity, residual stresses, and the formation of brittle phases within the welded zone further increase the susceptibility of steel structures to in-service failure [12–14]. Residual tensile stresses generated during welding, when combined with operational stresses and corrosive environments, can initiate stress corrosion cracking, which remains one of the primary causes of failure in oil and gas infrastructure [6, 15, 16].Although post-weld heat treatment (PWHT) is widely recognized for its benefits in stress relief and toughness improvement, current industrial practices provide limited guidance for simultaneously optimizing both mechanical properties and corrosion resistance in UNSG10350 carbon steel.

The fabrication of pipelines involves welding processes that produce heat-affected zones with varying hardness and microstructural characteristics. These regions often contain brittle, untemperedmartensite [17–19], which exhibits high sensitivity to crack initiation under corrosive conditions and cyclic loading. The adverse effects of residual stresses and unfavorable microstructures can be mitigated through post-weld heat treatment (PWHT), which improves material properties and corrosion resistance by reducing residual stresses and refining the microstructure [20–22].Tempering of steel is typically achieved by heating within the temperature range of 250–650 °C, transforming brittle martensite into more ductile tempered structures. This transformation enhances toughness while reducing susceptibility to chloride-induced stress corrosion cracking [23]. However, studies on the optimization of post-weld tempering parameters for UNSG10350 carbon steel in chloride-containing environments remain limited, particularly regarding the balance between mechanical strength and corrosion resistance.

2. MATERIALS AND METHODS

2.1 Materials

The materials used for this study were selected based on their availability within the local environment. The carbon steel pipe and E6013 welding electrode were procured from Chemz Limited, Warri, Delta State, Nigeria. Other materials and equipment used included an electronic weighing balance, muffle furnace, tongs, grinding machine, distilled water, ethanol, acetone, beakers, and emery papers. The chemical compositions of the carbon steel and welding electrode are presented in Table 1.

Table 1. Chemical Composition of UNSG10350 carbon steel and electrode

Element	C	Mn	P	S	Si	Cr	Ni	Cu	Mo	Fe
carbon Steel	0.342	0.61	0.0010	0.0029	0.233	0.144	0.178	0.075	0.050	98.36
E6013 Electrode	C	Mn	Si	S	P					
	≤0.12	0.3-0.6	≤0.35	≤0.35	≤0.040					

2.2. Preparation of coupons for corrosion testing

The carbon steel pipe was cut and machined into square sections measuring 10 mm × 10 mm with a thickness of 4 mm using a cutter and grinding machine. Two prepared samples were subsequently welded together to produce a specimen measuring 20 mm × 10 mm.The specimens were classified into two main groups: the as-welded (control) carbon steel pipe and the post-weld heat-treated (PWHT) carbon steel pipe. The PWHT specimens were tempered at temperatures of 300 °C, 450 °C, and 650 °C, respectively.

2.3. Preparation of Brine Solution

A 3.5 wt. % NaCl solution was prepared by dissolving the required amount of sodium chloride (NaCl) in 1000 cm^3 of distilled water. The solution was continuously stirred until the NaCl was completely dissolved, resulting in a homogeneous solution.

2.4. Welding Process

Carbon steel pipe samples measuring 20 mm × 10 mm, 170 mm × 15 mm, and 70 mm × 10 mm were prepared for corrosion measurements, tensile testing, and hardness testing, respectively. The samples were welded using the electric arc welding process.To prevent poor weld quality and porous weld surfaces, the metal samples were thoroughly cleaned with a wire brush to remove surface contaminants and defects before welding. The workpiece was placed on a flat surface, and the electrode was positioned in the electrode holder at an angle of 60°–80°. In accordance with the procedure described in [24], a butt weld was

produced by bringing the electrode into contact with the prepared samples.

2.5. Post Weld Heat treatment Process

The samples were preheated to 100 °C prior to welding to ensure the formation of a defect-free and durable weld joint. Post-weld heat treatment (PWHT) tempering processes were subsequently carried out at temperatures of 300 °C, 450 °C, and 650 °C, with a holding time of 1 h for each treatment condition, followed by air cooling to room temperature.

An SX-4-10 muffle furnace was used to heat-treat the samples at the specified tempering temperatures.

2.6. Mass loss

The weight-loss technique was employed to determine the mass loss and corrosion rates of the specimens. Prior to exposure to the corrosive medium, the specimens were carefully cleaned and weighed to obtain their initial masses. After each immersion period, the specimens were removed from the corrosive environment, and surface debris and corrosion products were cleaned using distilled water and ethanol before reweighing.The experiment was conducted over a total immersion period of 120 h, during which the specimens were weighed at intervals of 24 h under controlled conditions to evaluate mass loss. The corrosion rates of the specimens were subsequently determined from the measured mass reduction resulting from corrosion. Equation (1) was used to calculate the corrosion rate [25].

$$R_{corr} = \frac{8.76 \times 10^4 \times \Delta W}{\rho A t} \quad (1)$$

Where, R_{corr} is the corrosion rate (mm/year), ΔW is the Change in mass (g), ρ is the Density (g/cm3) (7.85 g/cm^3), A is the Area of exposed surface in cm^2 and t is the time in hours (hr).

2.7. Electrochemical Testing

The carbon steel weld coupon samples were immersed in the corrosive solution, leaving approximately 0.5 cm of the sample exposed above the solution surface. Prior to electrochemical testing, the working electrodes (carbon steel specimens) were polished using 600- and 1000-grit emery papers, followed by cleaning with distilled water and ethanol. The specimens were then dried using ethanol before testing. Electrochemical measurements were carried out in a conventional three-electrode corrosion cell using a VERSASTAT 300 DC potentiostat connected to V3 Studio software. Potentiodynamic polarization experiments were also performed using a Galvano stat corrosion system integrated with the E-Chem computer program. In the electrochemical cell setup, the carbon steel specimen served as the working electrode, a graphite rod was used as the counter electrode, and a saturated calomel electrode (SCE) served as the reference electrode. The impedance behavior of the aerated brine solution was measured for 300 s at 25 °C using a Luggin capillary connected to the electrochemical system. Electrochemical impedance spectroscopy (EIS) measurements were conducted at the corrosion potential (Ecorr) with a signal amplitude perturbation of 5 mV [26, 27]. The corrosion rate of the carbon steel pipe weld samples was determined from the Nyquist plots using Equation (2).

$$\text{Corrosion rate (mm/yr)} = \frac{0.00327 \times jcorr \times Ew}{D} \quad (2)$$

Where, jcorr is the corrosion current density (A/cm^2), Ew is the weight percent of carbon steel, and D is the metal density (g/cm^3).

2.8. SEM Morphological Characterization

All samples were prepared to appropriate dimensions to fit within the specimen chamber and were rigidly mounted on specimen holders known as specimen stubs. Prior to examination, the samples were coated with a thin layer of platinum, an electrically conductive material, using either low-vacuum sputter coating or high-vacuum evaporation techniques to improve surface conductivity and image quality.The scanning electron microscopy (SEM) analysis was carried out using a JEOLJSM-7600F field-emission scanning electron microscope. The SEM chamber operates under relatively high vacuum conditions with a short working distance, while the electron optical column is differentially pumped to maintain a sufficiently low vacuum at the electron gun. The high-pressure region surrounding the sample helps neutralize surface charge and enhances the secondary electron signal.Low-voltage SEM imaging was employed because the field-emission gun of the JEOLJSM-7600F is capable of producing high primary electron brightness and a small spot size, even at low accelerating voltages. This capability enables high-resolution imaging of the sample surface morphology.

3. RESULTS AND DISCUSSION

3.1. Mass loss Analysis

Figure 1 illustrates the weight loss of carbon steel weld samples after 5 days (120 h) of immersion in a brine solution. The investigated samples included the as-welded (control) specimen and post-weld heat-treated (PWHT) specimens tempered at 300 °C, 450 °C, and 650 °C.The results show that the as-welded sample

experienced a rapid increase in weight loss during the initial 70 h of immersion compared with the PWHT-treated samples. However, as the exposure period increased from 70 h to 120 h, the rate of weight loss for all samples gradually decreased. This reduction in weight loss is attributed to the formation of a protective surface film on the sample surfaces [28].Furthermore, the as-welded sample exhibited the highest overall weight loss, indicating greater susceptibility to corrosion. In contrast, the PWHT-treated samples showed lower weight losses, with corrosion resistance improving in the following order: PWHT-300 °C <PWHT-450 °C <PWHT-650 °C. The PWHT-650 °C specimen demonstrated the lowest weight loss and, therefore, the highest corrosion resistance among the tested samples.

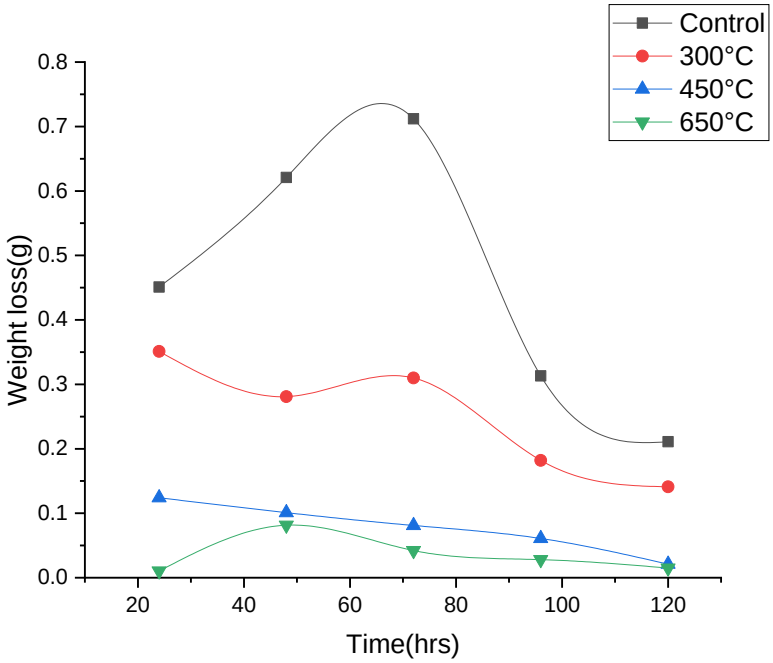

Figure 1. Weight loss in variation with time for the carbon steel welded pipe immersed in chloride induced environment

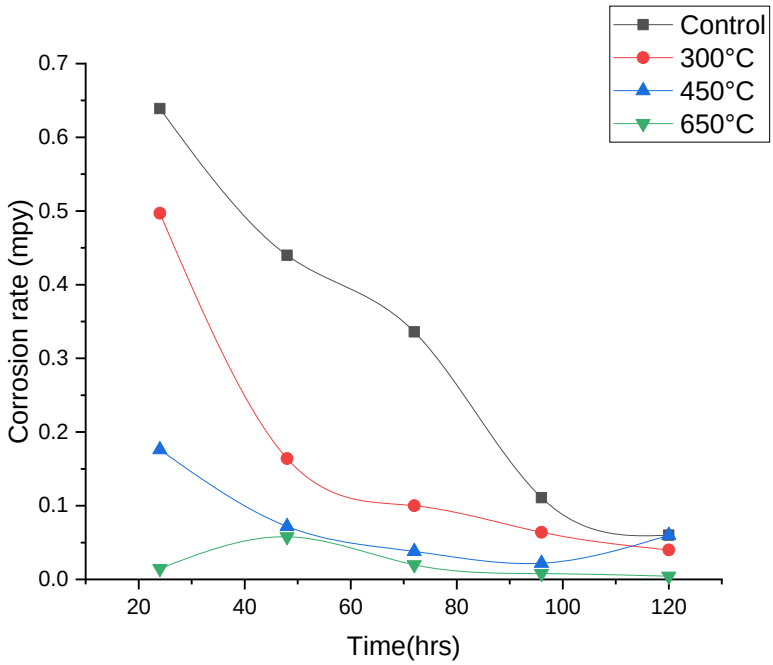

Figure 2. Corrosion rate in variation with time of the carbon steel weld immersed in chloride induced environment

Figure 2 illustrates the corrosion rates of the carbon steel weld samples after 5 days (120 h) of immersion in a brine solution. The investigated samples included the as-welded (control) specimen and the PWHT-treated specimens tempered at 300 °C, 450 °C, and 650 °C.The results revealed significant corrosion rates for all samples during the initial stage of exposure. The as-welded specimen exhibited the highest corrosion rate, with an optimum value of 0.639 mpy recorded within the first 24 h of immersion. However, the corrosion rates of all samples decreased progressively with increasing exposure time. This reduction is attributed to the interaction between the aggressive constituents of the brine environment and the transport mechanisms involved in the corrosion process, leading to the formation of a reddish-brown protective oxide layer on the sample surfaces. The protective layer partially inhibited further surface attack, thereby reducing the corrosion rate [29].These findings are consistent with the work of Lazaro et al. [30], who reported that the corrosion rate of carbon steel decreases over time due to the development of protective barrier layers on the steel surface. Furthermore, the results demonstrated that the PWHT-650 °C sample exhibited the lowest corrosion rate among all the PWHT-treated specimens, indicating superior corrosion resistance compared with the PWHT-300 °C and PWHT-450 °C samples.

3.2. Electrochemical measurements

The electrochemical measurement was investigated with open circuit potential potentiodynamic polarization, and electrochemical impedance spectroscopy.

3.2.1. Open circuit potential (OCP)

Figure 3 illustrates the variation of open-circuit potential (EOCP) with immersion time in seawater at 25 °C for the as-welded and PWHT-treated carbon steel weld samples. The EOCP of the as-welded sample initially started at approximately −0.475 V and gradually shifted anodically before stabilizing after about 300 s. The initial behavior is attributed to the dissolution of air-formed oxide layers on the sample surface, indicating the onset of corrosion attack on the metal surface. In comparison, the PWHT-treated samples (PWHT-300 °C, PWHT-450 °C, and PWHT-650 °C) exhibited more positive initial EOCP values, although they also shifted anodically with time. The results further indicate that the EOCP became increasingly positive with increasing PWHT temperature. This positive shift is associated with the formation of a more stable oxide layer on the sample surface, which acts as a protective barrier against further corrosion by chloride ions (Cl^-) present in the saline environment [31].

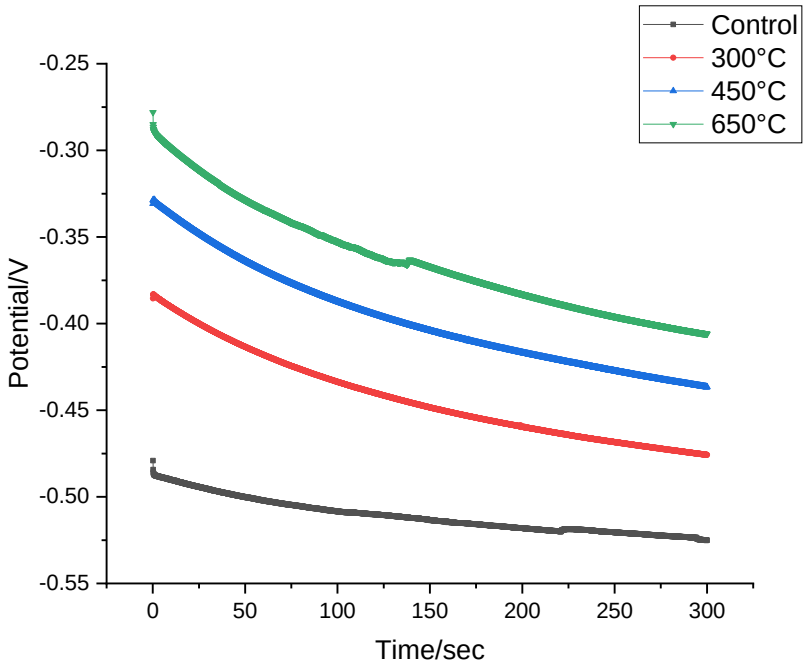

Figure 3. Open circuit potential curves of the carbon steel weld immersed in chloride induced environment

3.2.2. PotentiodynamicPolarization (PDP)

The potentiodynamic polarization behavior of the carbon steel weld samples was evaluated to investigate their anodic and cathodic corrosion processes [32]. Figure 4 presents the Tafel polarization curves for the as-welded and post-weld

heat-treated (PWHT) samples exposed to a chloride-containing environment. The results show that both the anodic and cathodic current densities of the PWHT-treated samples (PWHT-300 °C, PWHT-450 °C, and PWHT-650 °C) decreased significantly with increasing PWHT temperature compared with the as-welded sample.

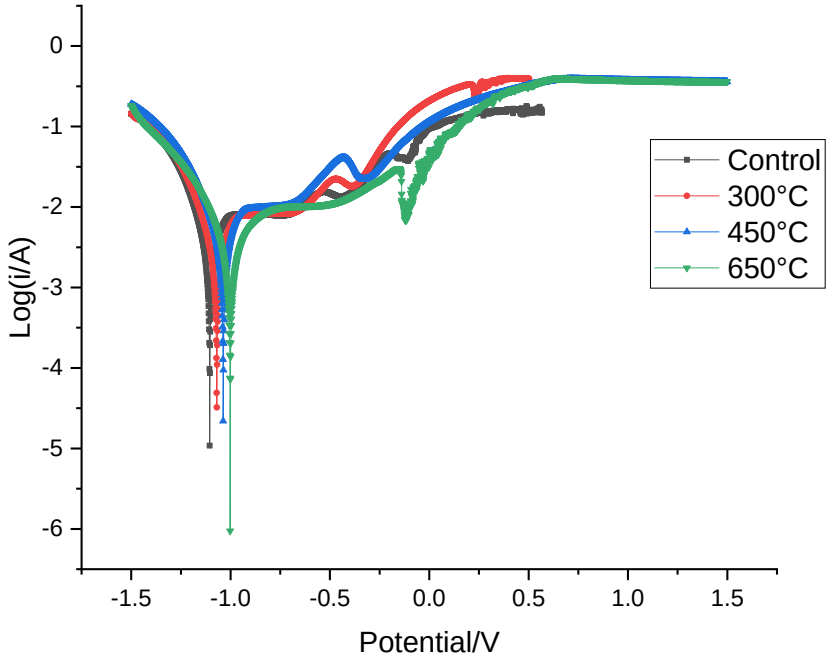

Figure 4. Tafel curves of as-welded and PWHT samples of the carbon steel weld immersed in chloride induced environment

The electrochemical corrosion parameters, including corrosion current density (jcorr), anodic and cathodicTafel slopes (βa and βc), and corrosion potential (Ecorr), were obtained from Tafel extrapolation and are summarized in Table 2. ThePWHT-treated samples exhibited lower corrosion current densities (jcorr) than the as-welded sample, indicating improved corrosion resistance. This improvement is attributed to the tempering process, which reduced ion exchange reactions occurring at the anodic and cathodic sites on the metal surface, as similarly reported by Ajide et al.[33].The corrosion rates of the as-welded, PWHT-300 °C, PWHT-450 °C, and PWHT-650 °C samples were 0.284, 0.126, 0.0864, and 0.0148 mpy, respectively. The reduction in corrosion rate after tempering is associated with the formation of a protective surface layer that inhibited further corrosion attack [33].

Table 2.Tafel data for the as-welded and PWHT of Carbon steel samples in brine solution

Samples	β_a ($mVdec^{-1}$)	β_c($mVdec^{-1}$)	Ecorr(V)	jcorr(μA/cm²)	Corrosion Rate (mpy)
As-welded	20.312	3.42	-4.104	8.621	0.284
300 ^{0}C	8.275	6.55	-2.84	2.528	0.126
450 ^{0}C	7.952	4.612	-2.44	2.284	0.0864
650 ^{0}C	3.838	2.631	-2.26	0.848	0.01483

3.2.3. Electrochemical impedance spectroscopy (EIS)

Figure 5 presents the electrochemical impedance spectroscopy (EIS) Nyquist plots of carbon steel pipe welds exposed to a chloride-containing environment for both the as-welded and PWHT-treated samples. The plots exhibit semicircular characteristics across the investigated frequency range, indicating charge-transfer-controlled corrosion behavior. Similar semicircular trends were observed for both the as-welded and PWHT samples [34]. However, the as-welded sample exhibited a smaller semicircle diameter compared with the PWHT-treated samples, indicating a lower charge-transfer resistance (Rct), as presented in Table 3.

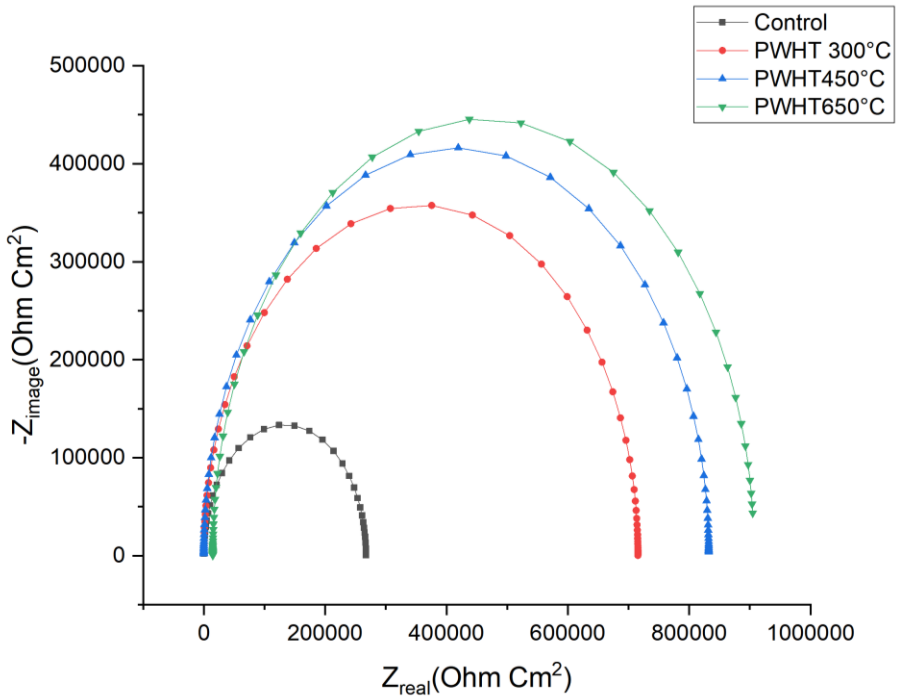

Figure 5. Nyquist curves of as-welded and PWHT samples of the carbon steel pipe weld immersed in chloride induced environment

Table 3. Nyquist data for as-welded and PWHT samples of the carbon steel pipe weld immersed in chloride induced environment.

Samples	Rs(Ωm^2)	CPE Cdl(μF/cm²)	n	Rct (Ωm^2)
As-welded	0.00028	67.28	0.9996	1012
300 ^{0}C	0.0023	42.05	0.9947	2816
450 ^{0}C	0.0014	13.18	0.9888	3742
650 ^{0}C	0.008	4.28	0.9817	4826

The results in Table 3 further demonstrate that the PWHT-treated samples exhibited improved corrosion resistance relative to the as-welded sample. Additionally, the charge-transfer resistance increased progressively with increasing PWHT tempering temperature. The results also revealed that the PWHT process reduced the double-layer capacitance (Cdl) of the treated samples, as shown in Table 3. The observed variations in the electrochemical properties of the samples are attributed to changes in the microstructure and mechanical properties caused by recrystallization during the PWHT process [24, 34].

The Nyquist data parameters are solution resistance (Rs), charge transfer resistance (Rct), surface heterogeneity measure (n), and constant phased element (CPE)

3.2.4. Surface Morphology

Figure 6(a–e) presents the surface morphologies of the as-received, as-welded, PWHT-300 °C, PWHT-450 °C, and PWHT-650 °C samples, respectively. Figure 6(a) shows a relatively smooth surface morphology, indicating that the as-received sample had not been exposed to a corrosive or degrading environment. In contrast,

Figure 6(b), which represents the as-welded sample, revealed localized corrosion attack characterized by pitting formation. The microstructure of the as-welded sample was predominantly composed of grain boundary ferrite [28].Compared with the as-welded condition, the post-weld heat-treated samples shown in Figure 6(c–e) exhibited increased grain sizes and the formation of tempered martensitic structures. These microstructural changes are attributed to recrystallization and grain growth resulting from the post-weld tempering process. Generally, grain size increases with increasing tempering temperature [35].The results further indicate that post-weld heat treatment significantly influenced the corrosion behavior of the samples. The larger grain size and tempered martensitic microstructure contributed to improved corrosion resistance. Consequently, the PWHT-650 °C sample exhibited superior corrosion resistance compared with the other samples due to its enhanced grain growth and more stable microstructure [36].

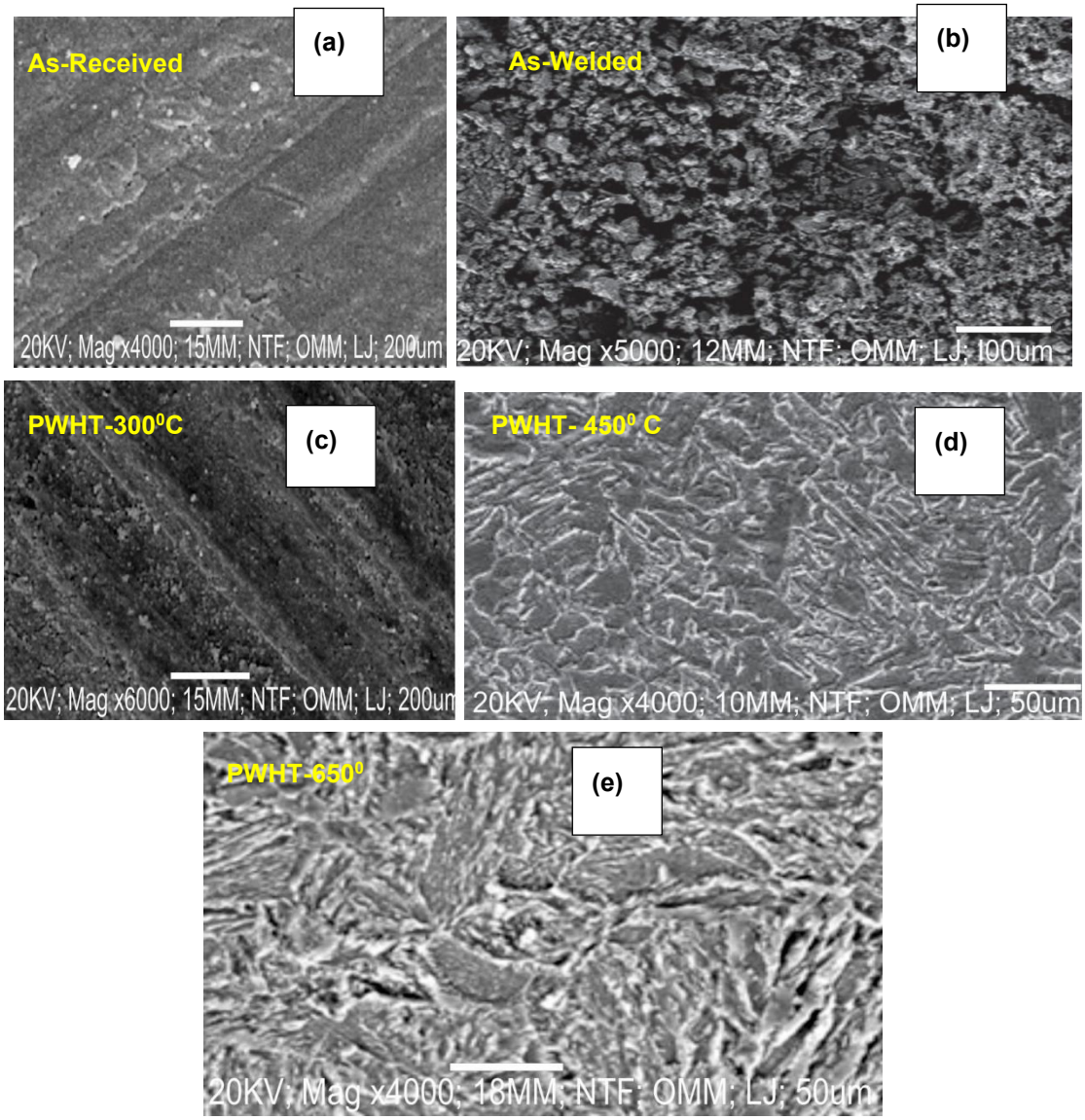

Figure 6 .SEM image of (a) As-received , (b) As-welded ,(c) PWHT-300⁰C , (d) PWHT- 450⁰C (e) PWHT- 650⁰C sample immersed in an induced chloride environment

4. CONCLUSION

The weight loss of the carbon steel weld samples in the chloride-rich environment decreased with increasing PWHT temperature. The as-welded sample exhibited the highest weight loss, particularly during the first 70 h of exposure. In contrast, the PWHT-650 °C sample demonstrated the lowest weight loss, which is attributed to the formation of a stable protective surface film. The PWHT-treated samples exhibited more positive and stable open-circuit potential (OCP) values compared with the as-welded sample, indicating enhanced resistance to chloride-induced corrosion due to the formation of a protective oxide layer on the sample surface.

Furthermore, PWHT significantly reduced the corrosion current densities and corrosion rates of the samples. The corrosion rate decreased from 0.284 mpy for the as-welded sample to 0.0148 mpy for the PWHT-650 °C sample. This improvement is associated with increased surface passivation and reduced electrochemical activity at higher tempering temperatures. The electrochemical impedance spectroscopy (EIS) Nyquist plots revealed larger semicircle diameters for the PWHT-treated samples, indicating higher charge-transfer resistance (Rct). The increase in Rct and the corresponding decrease in double-layer capacitance (Cdl) with increasing tempering temperature further confirmed the improved corrosion resistance and enhanced surface stability

of the PWHT-treated samples.SEM analysis revealed that the as-welded sample was predominantly characterized by grain boundary ferrite, whereas the PWHT-treated samples developed tempered martensitic structures with increasing grain size as the tempering temperature increased. Overall, the application of post-weld heat treatment at 650 °C resulted in significant improvements in both corrosion resistance and mechanical performance of the carbon steel welds in chloride-rich environments. These improvements are attributed to stress relief, microstructural refinement, carbide redistribution, and the formation of protective surface films.

Conflict of interest

The authors report no competing interest to this study

5. REFERENCES

[1] K. Lahiri. (2017). Applied metallurgy and corrosion control. In Indian Institute of Metals Series. Springer Singapore. https://doi.org/10.1007/978-981-10-4684-1

[2] U. Tadama, & M. Tadama. (2024). Design basis and parametric criteria for offshore oil and gas material selection and consideration: A review. Journal of African Resilience and Advancement Research, 6(2), 175–194.

[3] S.A. Atta-Agyemang, M. A. Kesse, P. Kah, & J. Martikainen. (2016). Improvement of strength and toughness: The effect on the weldability of high-strength steels used in offshore structures. Proceedings of the Institution of Mechanical Engineers, Part B: Journal of Engineering Manufacture, 231(3), 369–376. https://doi.org/10.1177/0954405415600366

[4] O. S. Odebiyi, S. M. Adedayo, L. A. Tunji, & M. O. Onuorah. (2019). A review of weldability of carbon steel in arc-based welding processes. Cogent Engineering, 6(1). https://doi.org/10.1080/23311916.2019.1609180

[5] R. Francis,& G. Byrne. (2021). Duplex stainless steels—Alloys for the 21st century. Metals, 11(5), 836. https://doi.org/10.3390/met11050836

[6] E. A. Krivonosova. (2018). A review of stress corrosion cracking of welded stainless steels. OALib, 5(5), 1–41. https://doi.org/10.4236/oalib.1104568

[7] W. Li, R. Cao, L. Xu, & L. Qiao. (2021). The role of hydrogen in the corrosion and cracking of steels—A review. Corrosion Communications, 4, 23–32. https://doi.org/10.1016/j.corcom.2021.10.005

[8] M. Vakili, P. Koutník, J. Kohout, & Z. Gholami. (2024). Analysis, assessment, and mitigation of stress corrosion cracking in austenitic stainless steels in the oil and gas sector: A review. Surfaces, 7(3), 589–642. https://doi.org/10.3390/surfaces7030040

[9] M. S. Khan, M. Soleimani, A. R. H. Midawi, I. Aderibigbe, Y. N. Zhou, & E. Biro. (2023). A review on heat affected zone softening of dual-phase steels during laser welding. Journal of Manufacturing Processes, 102, 663–684. https://doi.org/10.1016/j.jmapro.2023.07.059

[10] H. B. Zhang, Z. W. Wang, P. Xue, J. H. Li, W. G. Wang, H. Zhang, D. R. Ni, F. C. Liu, B. L. Xiao, & Z. Y. Ma. (2024). Eliminating heat-affected zone of nuclear heat-resistant steel joint via low-temperature friction stir welding. Materials Science and Engineering: A, 916, 147340. https://doi.org/10.1016/j.msea.2024.147340

[11] Z. Li, Z. Fu, L. Wei, & B. Ji. (2025). Effect of heat-affected zone on electrochemical corrosion behavior of welded joint with multi-metallographic structure zone. Corrosion Science, 251, 112935. https://doi.org/10.1016/j.corsci.2025.112935

[12] M. N. James. (2011). Residual stress influences on structural reliability. Engineering Failure Analysis, 18(8), 1909–1920. https://doi.org/10.1016/j.engfailanal.2011.06.008

[13] K. Masubuchi. (2013). Analysis of welded structures: Residual stresses, distortion, and their consequences (Vol. 33). Elsevier. https://doi.org/10.1016/B978-0-08-022714-6.50020-4

[14] M. C. Zondi. (2014). Factors that affect welding-induced residual stress and distortions in pressure vessel steels and their mitigation techniques: A review. Journal of Pressure Vessel Technology, 136(4). https://doi.org/10.1115/1.4026564

[15] M. V. Kumar, V. Balasubramanian, S. Rajakumar, & S. K. Albert. (2015). Stress corrosion cracking behaviour of gas tungsten arc welded super austenitic stainless steel joints. Defence Technology, 11(3), 282–291. https://doi.org/10.1016/j.dt.2015.05.003

[16] R. Yadav, A. Kumar, G. P. Chaudhari, & A. G. Paradkar. (2022). Mechanical and stress corrosion cracking behavior of welded 5059H116 alloy. Corrosion Science, 206, 110528. https://doi.org/10.1016/j.corsci.2022.110528

[17] S. Papaefthymiou. (2021). Industrial pipeline welding. In Welding Technology (pp. 387–418). https://doi.org/10.1007/978-3-030-63986-0_12

[18] M. P. Singh, D. K. Shukla, R. Kumar, & K. S. Arora. (2020). The structural integrity of high-strength welded pipeline steels: A review. International Journal of Structural Integrity, 12(3), 470–496. https://doi.org/10.1108/IJSI-05-2020-0051

[19] N. Schroeder, M. Rhode, & T. Kannengiesser. (2024). Influence of microalloying on precipitation behavior and notch impact toughness of welded high-strength structural steels. Welding in the World, 68(10), 2647–2659. https://doi.org/10.1007/s40194-024-01796-8

[20] B. Huang, J. Liu, S. Zhang, Q. Chen, & L. Chen. (2020). Effect of post-weld heat treatment on the residual stress and deformation of 20/0Cr18Ni9 dissimilar metal welded joint by experiments and

simulations. Journal of Materials Research and Technology, 9(3), 6186–6200. https://doi.org/10.1016/j.jmrt.2020.04.022

[21] D. Tomerlin, D. Marić, D. Kozak, & I. Samardžić. (2023). Post-weld heat treatment of S690QL1 steel welded joints: Influence on microstructure, mechanical properties and residual stress. Metals, 13(5), 999. https://doi.org/10.3390/met13050999

[22] O. Falodun, S. Oke, & M. Bodunrin. (2025). A comprehensive review of residual stresses in carbon steel welding: Formation mechanisms, mitigation strategies, and advanced post-weld heat treatment techniques. The International Journal of Advanced Manufacturing Technology, 136(10), 4107–4140. https://doi.org/10.1007/s00170-025-15088-8

[23] D. C. Saha, E. Biro, A. P. Gerlich, & Y. Zhou. (2016). Effects of tempering mode on the structural changes of martensite. Materials Science and Engineering: A, 673, 467–475. https://doi.org/10.1016/j.msea.2016.07.092

[24] S. O. Okuma,& B. U. Oreko. (2024). Assessment of corrosion resistance potentials of welded and tempered UNSG10400 carbon steel in a seawater environment. Chemistry Africa, 7(5), 2767–2775. https://doi.org/10.1007/s42250-024-00922-5

[25] R. W. Revie,& H. H. Uhlig. (2025). Corrosion and corrosion control. John Wiley & Sons. https://doi.org/10.1002/9780470277270

[26] S. B. Ade. (2022). Inhibiting effect of natural plant leaves extract used as green corrosion inhibitor for mild steel in acidic media. International Journal for Research in Applied Science and Engineering Technology, 10(3), 136–147. https://doi.org/10.22214/ijraset.2022.40582

[27] S. Sair, A. Oushabi, K. Nehhale, Y. Abboud, O. Tanane, & A. El Bouari. (2018). Date palm waste extract as corrosion inhibitor for 304 stainless steel in 1 M HCl solution. International Journal of Electrochemical Science, 13, 10642–10653. https://doi.org/10.20964/2018.11.38

[28] S. A. Widyanto, A. Suprihanto, & M. A. Solikhin. (2025). The effect of heat treatment on the corrosion rate of medium carbon steel in seawater from the North Coast of Java. International Research Journal of Innovations in Engineering and Technology, 9(11), 275–279. https://doi.org/10.47001/IRJIET/2025.911035

[29] M. M. El-Naggar. (2006). Effects of Cl^-, NO_3^- and SO_4^{2-} anions on the anodic behavior of carbon steel in deaerated 0.50 M $NaHCO_3$ solutions. Applied Surface Science, 252(18), 6179–6194. https://doi.org/10.1016/j.apsusc.2005.08.025

[30] A. F. Lazaro, S. S. M. Tavares, G. Perez, R. T. Batista, & J. A. C. Velasco. (2023). Evaluation of post weld heat treatments and susceptibility to sulfide stress corrosion cracking of simulated HAZ in forged supermartensitic stainless steel UNSS41427. Engineering Failure Analysis, 152, 107494. https://doi.org/10.1016/j.engfailanal.2023.107494

[31] W. Zhang,& G. S. Frankel. (2003). Transitions between pitting and intergranular corrosion in AA2024. ElectrochimicaActa, 48(9), 1193–1210. https://doi.org/10.1016/S0013-4686(02)00828-9

[32] S. Chinnappan, S. Kandasamy, S. Arumugam, K.-K. Seralathan, S. Thangaswamy, & G. Muthusamy. (2017). Biomimetic synthesis of silver nanoparticles using flower extract of Bauhinia purpurea and its antibacterial activity against clinical pathogens. Environmental Science and Pollution Research, 25(1), 963–969. https://doi.org/10.1007/s11356-017-0841-1

[33] O. O. Ajide, O. O. Anifalaje, I. G. Akande, & et al. (2023). Effect of post-weld heat-treatment on corrosion and microstructure properties of electric arc welded mild steels. Portugaliae Electrochimica Acta, 41(1), 47–56. https://doi.org/10.4152/pea.2023410104

[34] Y. Zhao, C. Dong, Z. Jia, J. You, J. Tan, S. Miao, & Y. Yi. (2021). Microstructure characteristics and corrosion resistance of friction stir welded 2205 duplex stainless steel. Advances in Materials Science and Engineering, 2021. https://doi.org/10.1155/2021/8890274

[35] S. O. Seidu,& B. J. Kutelu. (2013). Influence of heat treatment on the microstructure and hardness property of inoculated grey cast iron. International Journal of Engineering and Technology, 3(9), 888–892.

[36] G. H. Aydoğdu,& M. K. Aydinol. (2006). Determination of susceptibility to intergranular corrosion and electrochemical reactivation behaviour of AISI316L type stainless steel. Corrosion Science, 48(11), 3565–3583. https://doi.org/10.1016/j.corsci.2006.01.003

IZVOD

ELEKTROHEMIJSKA PROCENA OTPORNOSTI NA KOROZIJU ZAVARA OD UGLJENIČNOG ČELIKA PWHTUNSG10350 U SIMULIRANOJ MORSKOJ VODI

Ova studija istražuje efekat termičke obrade nakon zavarivanja (PWHT) na ponašanje korozije zavarene cevi od ugljeničnog čelika (CS) u slanom okruženju koje sadrži hlorid na 25 °C. Korozija zavarenog (kontrolnog) uzorka upoređena je sa korozijom uzoraka tretiranih PWHT na 300 °C, 450 °C i 650 °C korišćenjem gravimetrijskih (gubitak mase) merenja i elektrohemijskih tehnika, uključujući potencijal otvorenog kola (OCP), potenciodinamičku polarizaciju (PDP) i elektrohemijsku impedansnu spektroskopiju (EIS). Rezultati gubitka mase dobijeni tokom 120 sati potapanja pokazali su da je zavareni uzorak doživeo najveću degradaciju. Brzo povećanje gubitka težine primećeno je tokom ranog perioda izlaganja (do približno 70 sati), nakon čega je usledilo smanjenje stope gubitka mase za sve uzorke pri dužim vremenima potapanja. Ovo ponašanje se pripisuje formiranju zaštitnog površinskog filma. Slično tome, brzine korozije su se smanjivale sa povećanjem vremena potapanja, verovatno zbog akumulacije produkata korozije koji su delimično inhibirali dalji napad. Merenja OCP-a su pokazala da su se uzorci tretirani PWHT-om pomerili ka pozitivnijim potencijalima u odnosu na stanje zavarenog stanja, što ukazuje na poboljšanu stabilnost površine povezanu sa formiranjem oksidnog sloja. Merenja PDP-a su dodatno potvrdila poboljšanu otpornost na koroziju nakon PWHT-a, sa brzinama korozije smanjenim na 0,126, 0,0864 i 0,0148 mm•god^{-1} za uzorke tretirane na 300 °C, 450 °C i 650 °C, respektivno. EISNyquist-ovi dijagrami su pokazali povećanje otpora prenosu naelektrisanja sa povećanjem temperature PWHT-a, praćeno smanjenjem dvoslojnog kapaciteta, što ukazuje na poboljšanu međupovršinsku zaštitu. SEM posmatranja su potvrdila elektrohemijske i gravimetrijske rezultate: zavarena površina je pokazala lokalizovano udubljivanje, dok je PWHT podstakla mikrostrukturnu evoluciju ka otpuštenom martenzitu i rastu zrna, što je rezultiralo značajno poboljšanom otpornošću na koroziju, posebno kod uzorka obrađenog PWHT-om na 650 °C. Generalno, PWHT, posebno na 650 °C, značajno je poboljšao otpornost na koroziju zavarenih spojeva od ugljeničnog čelika u sredinama koje sadrže hloride.

Ključnereči: *zavar ugljeničnog čelika, zavarljivost, PWHT, krtost, osetljivost*

Naučni rad
Rad primljen: 29.03.2026.
Rad korigovan: 11.05.2026.
Rad prihvaćen: 06.07.2026.

Prof. Benjamin U. Oreko https://orcid.org/0000-0002-7441-5722
Dr. Silas O. Okuma https://orcid.org/0000-0002-5735-6855